Comparative Analysis of Two Modulation Strategies for an Active Buck–Boost Inverter

Yu Tang, *Member, IEEE*, Fei Xu, *Student Member, IEEE*, Yang Bai, and Yaohua He

***Abstract*—The inverter used in the new energy power generation system should have the ability to adapt a wide range of dc input voltage. Based on the active buck–boost inverter, which consists of a full bridge and boost ac/ac part, two modulation methods are compared: constant boost ratio modulation and dual-mode modulation. Along with the relationship of the input dc voltage and the reference ac voltage, the converter completes buck or boost inversion with different equivalent circuits and there are fewer switches working at high frequency in dual-mode modulation, which is in favor of the system with high efficiency. The current of the inductor and the current stress of the switches are analyzed in this paper. Experimental results are presented to verify that the proposed topology can achieve the dual-mode operation with a wide range of input voltage.**

***Index Terms*—Buck–boost inverter, constant boost ratio modulation, dual-mode modulation, wide input.**

I. Introduction

With the development of the new energy, more and more attention is paid to inverters that can convert the dc voltage into ac voltage. According to whether there is isolation, the inverter can be divided into isolated and nonisolated type [1]–[3].

The isolated type with a transformer has a bigger volume and a higher cost, which is a disadvantage for the new energy power generation system [4], [5]. Influenced by the light, temperature, etc., the output voltage range of the PV cell is very wide [6], [7]. The output voltage of the single fuel cell is very low. If too many cells are in series, the voltage sharing is difficult to realize. So the inverters should have the ability to boost the input voltage [8].

The nonisolated inverters also can be divided into single-stage inverters and multistage inverters [9]–[11]. Boost cascaded inverters and buck–boost cascaded inverters are typical two-stage inverters [12], [13]. The two-stage structure has many inductors and capacitors, which are not suitable for integration. The dc bus needs a big electrolytic capacitor, which reduces the power density, is aging easily, and has a short service life. On the other hand, the cascaded structure which has poor stability and low efficiency is unfavorable to the new energy power generation system [14], [15]. The single-stage inverters, which have the ability to boost the input voltage, may reduce the system volume and improve power density. Z-source inverter, which can be viewed as a quasi-single-stage inverter, takes the advantage of the passive network to boost voltage and allows shoot through situation in bridge legs [16], [17]. But the drawbacks of high Z-source capacitor voltage stress and huge inrush surge may influence the efficiency, and vast passive components will also go against integration. Dual-boost inverter which has the advantage such as simple structure was introduced in [18], and a half-cycle modulation strategy was discussed. However, the efficiency of a dual-boost inverter is still low. Wu *et al.* [19] present a family of high-efficiency single-stage dc/ac inverter, only one power stage works in high-frequency stage at any time, which can reduce switching losses. Nonetheless, the passive components still cannot be decreased.

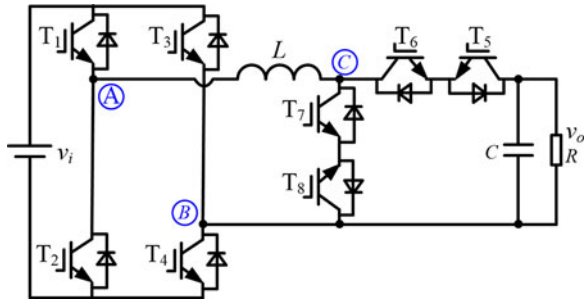

Fig. 1. Topology of the proposed active buck–boost inverter.

As shown in Fig. 1, Tang *et al.* [20] proposed a novel active buck–boost inverter. The converter is composed of a full bridge and a boost ac/ac structure and two parts share an inductor and a capacitor, which can boost the voltage, performs the voltage buck and boost conversion in a quasi-single-stage inverter, and has the advantages of compact structure, improved power density, and efficiency without utilization of a line-frequency transformer and additional passive elements. The duty ratio of the switches ($T_5 \sim T_8$) is determined by the relationship between the input voltage and the peak value of the output voltage reference to achieve a stable ac output. When the dc input voltage is stable, the duty ratio of the switches ($T_5 \sim T_8$) is also constant. In this paper, this modulation is called constant boost ratio modulation. As the unipolar Sine wave pulse width modulation (SPWM) is applied to the full bridge, the full bridge

Manuscript received May 18, 2015; revised August 09, 2015; accepted September 17, 2015. Date of publication September 29, 2015; date of current version June 24, 2016. This work was supported by the National Natural Science Foundation of China under Grant 51307083, the National Natural Science Foundation of Jiangsu province under Grant BK20130795, Open Fund from the Jiangsu Key Laboratory of New Energy Generation and Power Conversion under Grant ZAB11002-02, and the Priority Academic Program Development of Jiangsu Higher Education Institutions. Recommended for publication by Associate Editor Y. Liu.

The authors are with the Jiangsu Key Laboratory of New Energy Generation and Power Conversion, College of Automation Engineering, Nanjing University of Aeronautics and Astronautics, Nanjing 211106, China (e-mail: ty8025@hotmail.com; xuf_xuf@163.com; hello9272@163.com; hyhnuaa@126.com).

Color versions of one or more of the figures in this paper are available online at http://ieeexplore.ieee.org.

Digital Object Identifier 10.1109/TPEL.2015.2483906

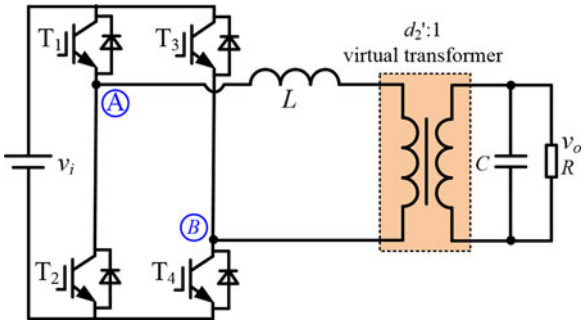

Fig. 2. Equivalent circuit of the proposed active inverter.

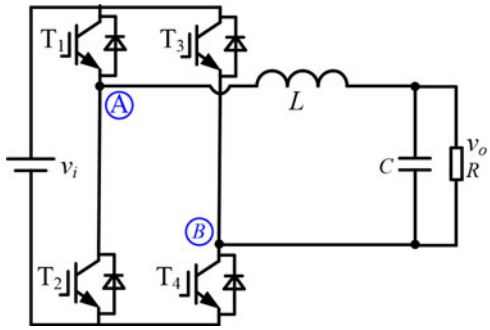

Fig. 3. Equivalent circuit under buck mode.

works in the buck mode and the boost ac/ac part must achieve a large boost ratio to maintain the output voltage when the input voltage is low. So the inductor current and the switches current stress are high. In addition, there are four switches working at high frequency in this modulation mode. So the switching loss is large and the efficiency of the inverter is low.

According to the relationship between the input voltage and the reference of output voltage, the time-sharing dual-mode modulation can help the inverter to work in different modes to reduce the number of the switches which work in high frequency. Thus, lower switching cost and higher efficiency can be obtained [21], [22]. But this modulation method is applied in the boost cascaded inverter which has the problems mentioned above. In this paper, the dual-mode modulation is applied in the inverter as shown in Fig. 1. Thus, the switching loss is reduced and the efficiency of the inverter is improved.

This paper is organized as follows: Sections II and III give the principle of constant boost ratio modulation and the dual-mode modulation, respectively. Section IV analyzes the current stress of inductor and power switches and gets a comparison between the two modulations. Simulation and experimental results are presented in Section V. Finally, Section VI concludes this paper.

II. Principle of Constant Boost Ratio Modulation

From the point of view of voltage gain, the boost ac/ac part can be treated as a "virtual transformer" whose boost ratio is $1/d_2'$(d_2' is the duty ratio of the switch T_5 or T_6 when they work in high frequency). The equivalent circuit is presented in Fig. 2. The relationship between the dc input and the ac output voltage of the converter is

$$\frac{V_{\rm op}}{v_i} = \frac{M}{1-d_2} = \frac{M}{d_2'} \tag{1}$$

where v_i is the input voltage, $V_{\rm op}$ is the peak value of the output voltage v_o, and M is the modulation ratio. d_2 is the duty ratio of the switch T_7 or T_8 when they work in high frequency. It is noted that the active buck–boost inverter is a bidirectional converter, the current can flow through the inductor bidirectionally in one duty cycle, and the inverter will operates in CCM and never runs into DCM.

When $v_i > V_{\rm op}$, the boost ac/ac part does not work, $d_2' = 1$. When $v_i < V_{\rm op}$, the full bridge part works with full modulation ratio ($M = 1$), and outputs the equivalent sine voltage whose peak value is v_i ($v_{\rm AB} = v_i \sin(\omega t)$) and the boost ac/ac part works as a "virtual transformer" to boost the voltage

$$d_2' = 1 - d_2 = \begin{cases} 1, & v_{\rm i} \geq V_{\rm op} \\ \dfrac{v_{\rm i}}{V_{\rm op}}, & v_{\rm i} < V_{\rm op} \end{cases}. \tag{2}$$

In this way, as the full bridge works under the unipolar SPWM modulation, there are always two switches operating at high frequency. For boost ac/ac part, if a pair of switches is always ON, the other one pair is complementary ON at high frequency. So there are four switches in total operating at high frequency that are not conducive to improve the efficiency of the converter.

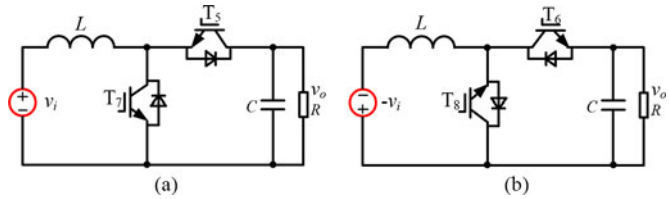

Fig. 4. Equivalent circuits under boost mode. (a) Positive period ($v_o > 0$). (b) Negative period ($v_o < 0$).

III. Principle of Dual-Mode Modulation

A. Buck Mode

When $v_i > v_o$, it will operate in buck mode in which T_5 and T_6 will be always ON and T_7 and T_8 will be always OFF. The equivalent circuit is shown in Fig. 3. Now, the whole circuit is equivalent to a full-bridge inverter. The relationship between v_i and v_o is

$$\frac{v_o}{v_i} = M \sin(\omega t) \tag{3}$$

where $v_o = V_{\rm op} \sin(\omega t)$.

So the duty ratio of the switch T_1 or T_3 when they work in high frequency is

$$\frac{V_{\rm op} \sin(\omega t)}{v_i} = d_1(t). \tag{4}$$

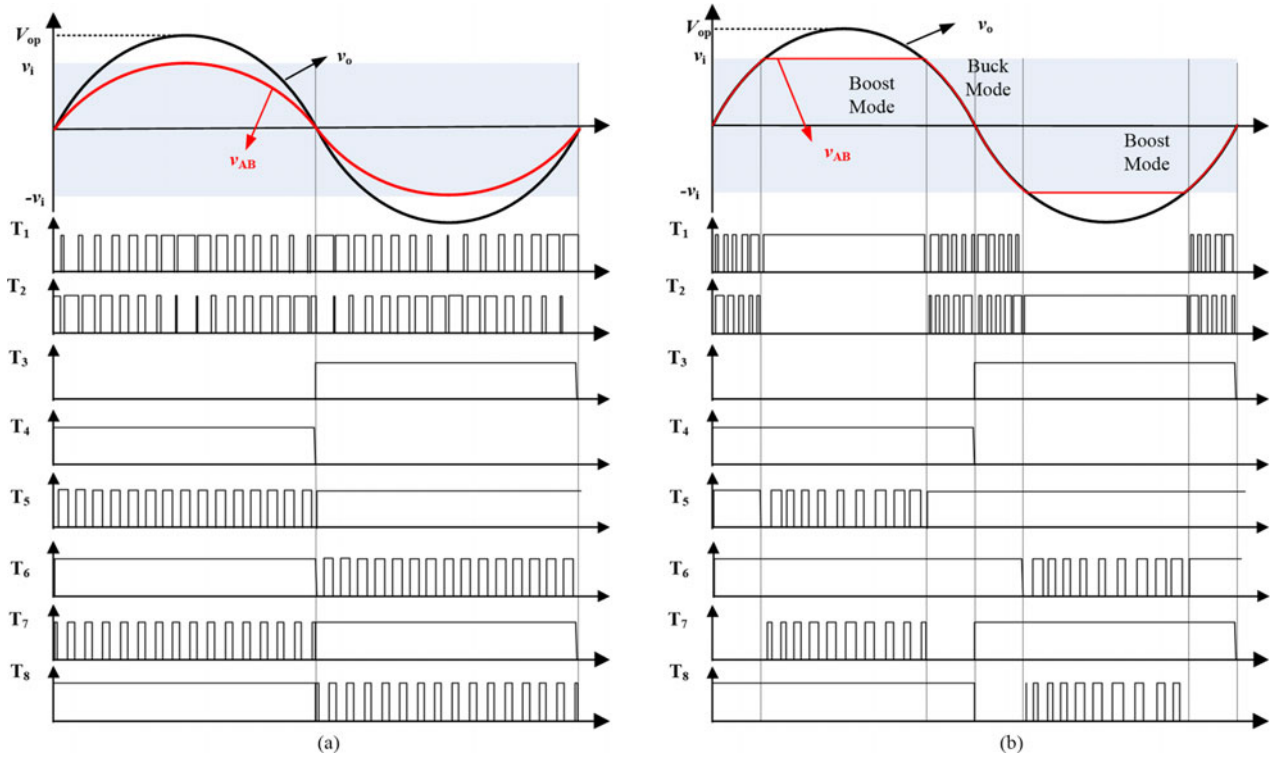

Fig. 5. Comparison of the modulation strategy. (a) Constant boost ratio. (b) Dual mode.

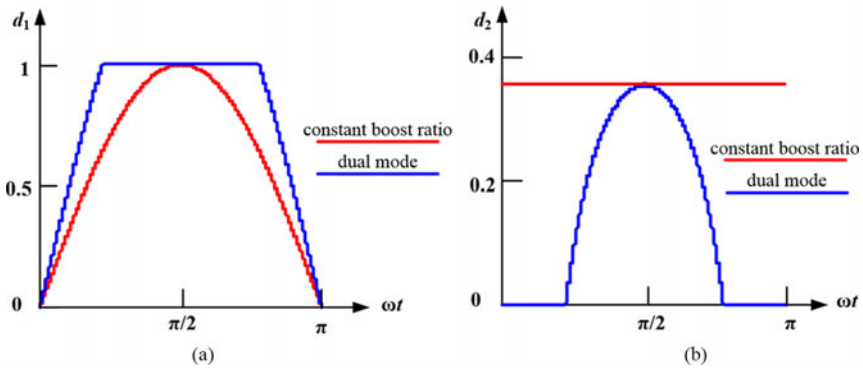

Fig. 6. Comparison of the duty ratio. (a) Duty ratio d_1. (b) Duty ratio d_2.

B. Boost Mode

When $v_i < v_o$, it will operate in boost mode in which the full bridge operates at a constant output state. When the modulation wave is higher than zero, T_1 and T_4 are always ON, and the output of the full bridge is v_i. Otherwise, T_2 and T_3 are always ON, and the output is $-v_i$. The boost ac/ac part works to boost the output voltage of the full bridge with its switches, whose duty ratio varies with the output voltage, operating in high frequency. The equivalent circuits of the two states are shown in Fig. 4.

In this mode, the duty ratio of the switch T_5 or T_6 is

$$d_2'(t) = \frac{v_i}{v_o} = \frac{v_i}{V_{\text{op}} \sin(\omega t)}. \tag{5}$$

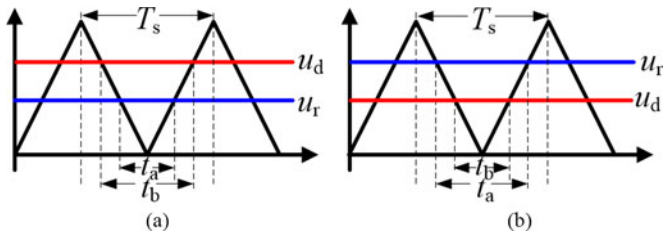

Fig. 7. Modulation waveforms. (a) $v_i > v_o$, (b) $v_i < v_o$.

So

$$d_2'(t) = 1 - d_2(t) = \begin{cases} 1, & v_i \geq v_o \\ \dfrac{v_i}{v_o}, & v_i < v_o \end{cases}. \tag{6}$$

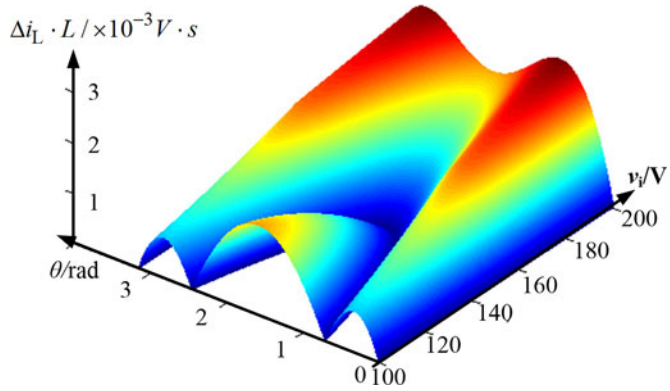

Fig. 8. Inductor current ripple in constant boost ratio modulation.

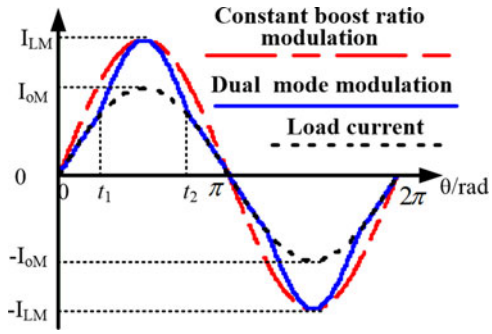

Fig. 9. Waveforms of inductor current.

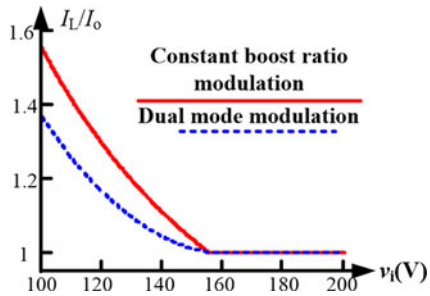

Fig. 10. Relationship between the rms value of the inductor current and the load current.

Thus, if $v_i > V_{\rm op}$, the inverter will always work in buck mode. If $v_i < V_{\rm op}$, the inverter will switch between buck mode and boost mode depending on the instantaneous output reference voltage.

Fig. 5 shows the comparison of the constant boost ratio modulation and the dual-mode modulation strategy. When $v_i < V_{\rm op}$, in constant boost ratio modulation, the boost ac/ac part always works in high frequency and ensures a constant boost ratio of the "virtual transformer," the full bridge part also works in high frequency and outputs an SPWM wave with full modulation ratio ($M = 1$) as shown in Fig. 5(a); while in dual-mode modulation, at any time, there is only one part works in high frequency as shown in Fig. 5(b). Compared with the constant boost ratio modulation, it can reduce switching loss. Fig. 6 shows the comparison of duty ratio d_1 [see Fig. 6(a)] and d_2 [see Fig. 6(b)] in two modulation strategies when $v_i = 100$ V and $V_{\rm op} = 155$ V. We can see that dual-mode modulation has larger d_1 and smaller d_2. The direct power transfer time of the buck converter and the boost converter is $d_1 T_s$ and $(1 - d_2)T_s$, respectively; therefore, dual-mode modulation has more direct power transfer time, which can improve the system efficiency.

TABLE I
INDUCTOR CURRENT RIPPLE UNDER TWO MODULATION MODE

Modulation mode	$v_i < v_o$	$v_o < v_i < V_{\rm op}$	$v_i > V_{\rm op}$
Constant boost ratio modulation	$di_L = \frac{(v_o - v_i)v_i T_s}{L V_{\rm op}}$	$di_L = \frac{(v_i - v_o)v_o T_s}{L V_{\rm op}}$	$di_L = \frac{(v_i - v_o)v_o T_s}{L v_i}$
Dual-mode modulation	$di_L = \frac{(v_o - v_i)v_i T_s}{L v_o}$	$di_L = \frac{(v_i - v_o)v_o T_s}{L v_i}$	$di_L = \frac{(v_i - v_o)v_o T_s}{L v_i}$

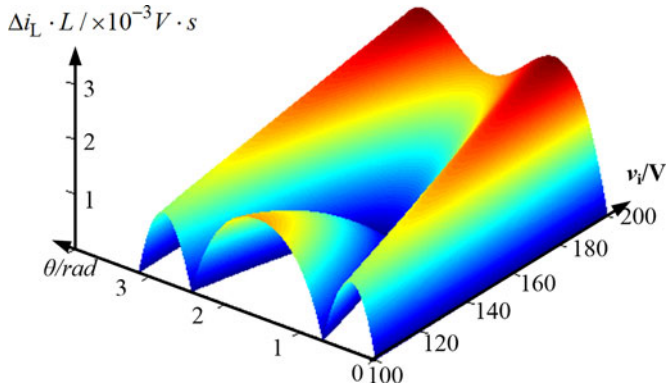

Fig. 11. Inductor current ripple under dual-mode modulation.

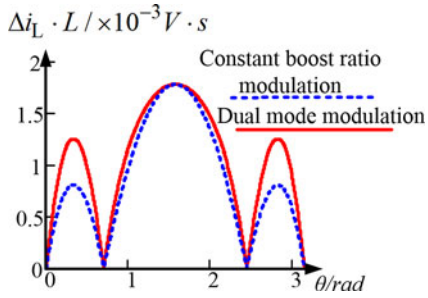

Fig. 12. Inductor current ripple comparison.

IV. Comparison of Two Modulations

The operating modes of the switches are different due to different modulation strategies. So the inductor current and the current stress of the switches are not the same.

A. Inductor Current

Due to the different equivalent boost ratio, the inductor current is also different.

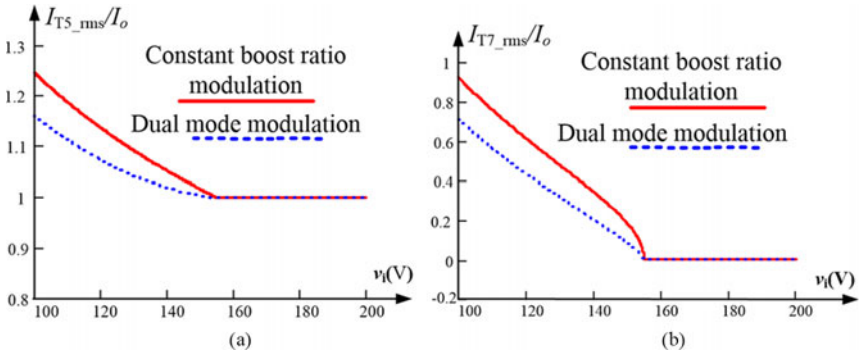

Fig. 13. Current rms value of switches. (a) T_5. (b) T_7.

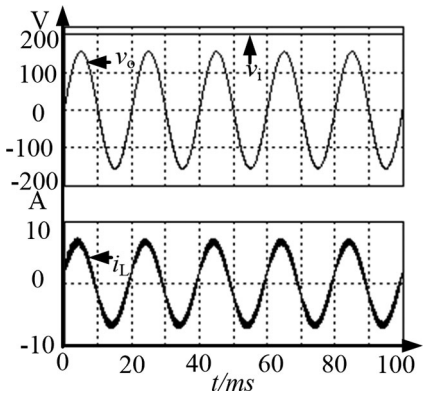

Fig. 14. Simulation waveforms under buck mode ($v_i = 200$ V).

1) Constant Boost Ratio Modulation: From the analysis above, when $v_i > V_{\rm op}$, the current of the inductor is equal to load current; whereas, when $v_i < V_{\rm op}$, the turns ratio of "the virtual transformer" is d_2', and the fundamental frequency component (the current ripple of the inductor is neglected) of the inductor current is equal to the current of the primary side of the transformer. So the current of the inductor can be given as follows:

$$i_L = \frac{i_o}{d_2'} = \begin{cases} i_o, & v_i \geq V_{\rm op} \\ \dfrac{i_o}{v_i/V_{\rm op}}, & v_i < V_{\rm op} \end{cases} \tag{7}$$

where i_o is the fundamental frequency component of the load current.

The current ripple of the inductor is

$$\Delta i_L = \frac{U_L \Delta T}{L} \tag{8}$$

where $u_L = v_{\rm AB} - v_{\rm CB}$.

When $v_i > V_{\rm op}$, the output of the full bridge $u_{\rm AB}$ is v_i and 0. So the inductor voltage u_L is $v_i - v_o > 0$ and $-v_o < 0$, and each action time is $T_s \times v_o/v_i$ and $T_s \times (1 - v_o/v_i)$, respectively. So

$$\Delta i_L = \frac{(v_i - v_o) v_o T_s}{L v_i}. \tag{9}$$

When $v_i < V_{\rm op}$, there are two cases as follows.

1) $v_i > v_o$: The modulation wave of the boost ac/ac part (u_d) is higher than the full bridge's (u_r) as shown in Fig. 7(a). During time interval t_a, $v_{\rm AB} = v_i$ and $v_{\rm CB} = v_o$, so $u_L = v_i - v_o > 0$. During time interval $t_b - t_a$, $v_{\rm AB} = 0$, $v_{\rm CB} = v_o$, so $u_L = -v_o < 0$. During time interval $T_s - t_b$, $v_{\rm AB} = 0$, $v_{\rm CB} = 0$, so $u_L = 0$. So the inductor current increases only in t_a time period. As $t_a = T_s \times M\sin(\omega t) = T_s \times \sin(\omega t) = T_s \times v_o/V_{\rm op}$, so

$$\Delta i_L = \frac{(v_i - v_o) v_o T_s}{L V_{\rm op}}. \tag{10}$$

2) $v_i < v_o$: The relationship of the modulation waves is shown in Fig. 7(b). During time interval t_b, $v_{\rm AB} = v_i$ and $v_{\rm CB} = v_o$, so $u_L = v_i - v_o < 0$. During time interval $t_a - t_b$, $v_{\rm AB} = v_i$ and $v_{\rm CB} = 0$, so $u_{\rm L} = v_{\rm i} > 0$. During time interval $T_s - t_a$, $v_{\rm AB} = 0$ and $v_{\rm CB} = 0$, so $u_L = 0$. Similarly, we can get

$$\Delta i_L = \frac{(v_o - v_i) v_i T_s}{L V_{\rm op}}. \tag{11}$$

Fig. 8 shows the relationship between the inductor current ripple and the output voltage. We can see that the inductor current ripple in buck mode is larger than in boost mode. The ripple becomes larger as the input voltage becomes higher.

2) Dual-Mode Modulation: Due to different operation modes, the equivalent circuits of the inverter are different, so the inductor current ripple is also different.

When $v_i > v_o$, the boost ac/ac part does not work, the current of the inductor is equal to load current. So

$$i_L = i_o. \tag{12}$$

When $v_i < v_o$, the boost ac/ac part work and can be treated as a transformer whose turns ratio is v_i/v_o. So the current of the inductor is equal to the current of the primary side of the transformer

$$i_L = \frac{i_o}{d_2'(t)} = \frac{i_o}{v_i/v_o}. \tag{13}$$

So

$$i_L = \frac{i_o}{d_2'(t)} = \begin{cases} i_o, & v_i \geq v_o \\ \dfrac{i_o}{v_i/v_o}, & v_i < v_o \end{cases}. \tag{14}$$

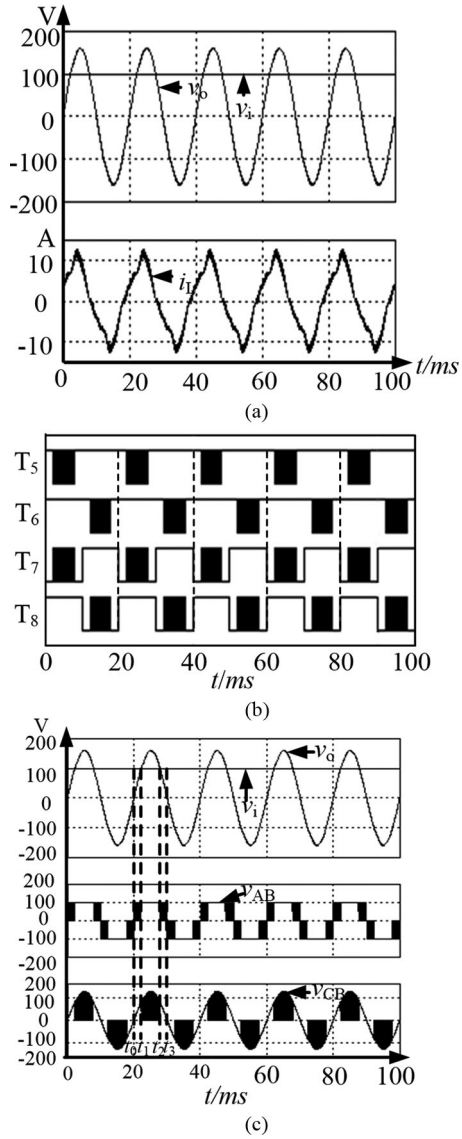

Fig. 15. Simulation waveforms in dual-mode modulation ($v_i = 100$ V). (a) Input and output voltage and inductor current. (b) Driving signals. (c) Inductor voltage.

Fig. 9 shows the relationship between the inductor current and the load current in two modulation modes when the input voltage is 100 V (the current ripple is neglected). We can see that the inductor current in dual-mode modulation is lower than in constant boost ratio modulation, which corresponds to the comparison results of the formula (7) and (14).

The rms value of the inductor current is

$$I_L = \sqrt{\frac{1}{2\pi}\int_0^{2\pi} i_L^2 \, d\theta}. \tag{15}$$

So we can get the relationship between the rms value of inductor current and the rms value of the load current (I_o) in different modulation as shown in Fig. 10. When the input voltage is lower than 155 V, the rms value of the inductor current in dual-mode modulation is lower than in constant boost ratio modulation. When the input voltage is higher than 155 V, they

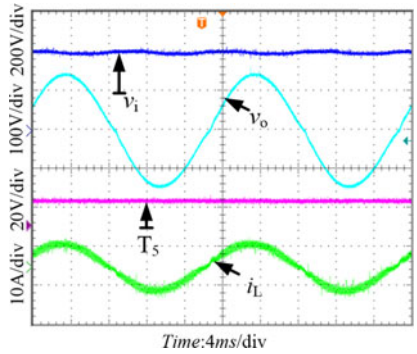

Fig. 16. Experimental waveforms under buck mode when the input voltage is 200 V.

are equal to load current. Normally, we should put the minimum input voltage in accordance with the maximum inductor current into consideration when designing the inductor. So in dual-mode modulation, thinner wires can be used. Thus, the volume of the inductor can be reduced.

When the inverter works in buck mode ($v_i > v_o$), the inductor voltage is $v_i - v_o$ and $-v_o$ and each action time is $T_s \times v_o/v_i$ and $T_s \times (1 - v_o/v_i)$, respectively. So

$$\Delta i_L = \frac{T_s(v_i - v_o)v_o}{Lv_i}. \tag{16}$$

When the inverter works in boost mode ($v_i < v_o$), the inductor voltage is v_i and $v_i - v_o$ and each action time is $T_s(1 - v_i/v_o)$ and $T_s v_i/v_o$, respectively. So

$$\Delta i_L = \frac{T_s(v_o - v_i)v_i}{Lv_o}. \tag{17}$$

Fig. 11 shows the inductor current ripple under dual mode modulation which is similar to Fig. 8. The Table. 1 displays a comparison of the inductor current ripple equations in different modulation modes.

As Table I shows when $v_i > V_{\rm op}$, the inductor has the same ripple because the equivalent circuits are the same. When $v_i < V_{\rm op}$, the ripple is larger in dual-mode modulation. Fig. 12 shows the comparison of the inductor current ripple in different modulation modes when the input voltage is 100 V, which corresponds to the theoretical analysis.

B. Current Stresses on Switches

The conduction time of each switch ($T_1 \sim T_4$) in full bridge part is half a line period. Once turned ON, the current of these switches is the same as the inductor current. As the inductor current in dual mode is lower, the current stress of these switches is lower than in constant boost ratio modulation. Once turned ON, the current of the switches ($T_5 - T_8$) is the same as the inductor current. So in constant boost ratio modulation

$$I_{T5\_\rm rms} = I_{T6\_\rm rms} = \sqrt{\frac{1}{\pi}\int_0^{\pi}\left(\left(\frac{i_o}{d_2'}\right)^2 \times d'\right)d\theta}$$

$$= \sqrt{\frac{1}{\pi d_2'}\int_0^{\pi} i_o^2 d\theta} \tag{18}$$

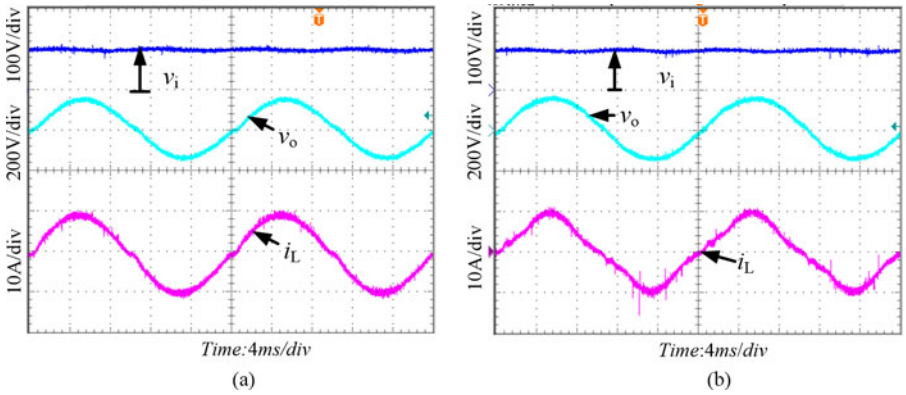

Fig. 17. Comparison of input and output voltage and the output current in different modulations. (a) Constant boost ratio modulation. (b) Dual-mode modulation.

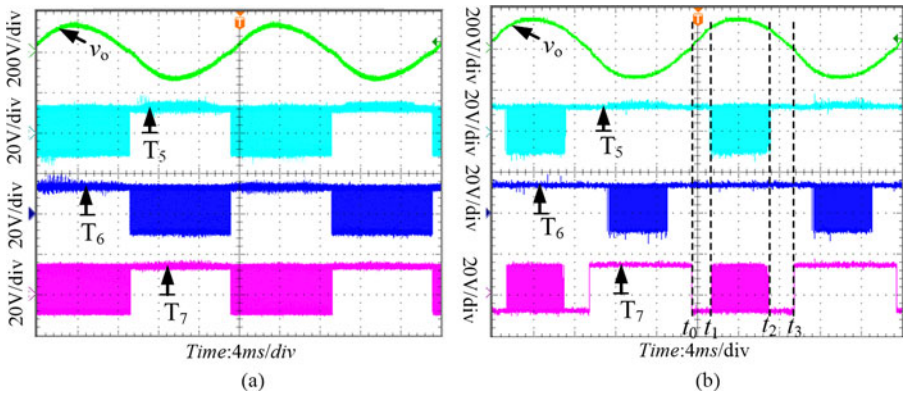

Fig. 18. Comparison of the driving signals in different modulations. (a) Constant boost ratio modulation. (b) Dual-mode modulation.

$$I_{T7\_\mathrm{rms}} = I_{T8\_\mathrm{rms}} = \sqrt{\frac{1}{\pi}\int_0^{\pi}\left(\left(\frac{i_o}{d_2'}\right)^2 \times (1-d_2')\right)d\theta}. \quad (19)$$

In dual-mode modulation, we can get

$$I_{T5\_\mathrm{rms}} = I_{T6\_\mathrm{rms}} = \sqrt{\frac{1}{\pi}\int_0^{\pi}\left(\left(\frac{i_o}{d_2'(\theta)}\right)^2 \times d_2'(\theta)\right)d\theta} = \sqrt{\frac{1}{\pi}\int_0^{\pi}\frac{i_o^2}{d_2'(\theta)}d\theta} \quad (20)$$

$$I_{T7\_\mathrm{rms}} = I_{T8\_\mathrm{rms}} = \sqrt{\frac{1}{\pi}\int_{\beta}^{\pi-\beta}\left(\left(\frac{i_o}{d_2'(\theta)}\right)^2 \times (1-d_2'(\theta))\right)d\theta} \quad (21)$$

where $\beta = \sin^{-1}(v_i/V_{\mathrm{op}})$.

Fig. 13 shows the comparison of the current stress of the switches T_5 and T_7 in two different modulations. When the input voltage is lower than 155 V, compared with constant boost ratio modulation, the current stress of the switches ($T_5 - T_8$) is lower in dual-mode modulation.

V. Simulation and Experimental Results

A. Simulation Results

The input voltage v_i : $100 - 200\ V$. The output voltage v_o is 110 V/50 Hz ac. The output load is pure resistive. The switching frequency $f_s = 20$ kHz, $L = 1$ mH, and $C = 20\ \mu$F.

Fig. 14 shows the output voltage and the inductor current waveforms under the condition $v_{\mathrm{i}} = 200$ V. When the input voltage is high, the inductor has small current but large current ripple. In Fig. 15, the input voltage is 100 V. The results show that the inverter can achieve smooth switching between two modes in dual-mode modulation, which corresponds to the theoretical analysis.

B. Experimental Results

To verify the theoretical analysis of the proposed converter, a 500-W prototype circuit is built in the laboratory. The system parameters in the experiment are the same as in Section V-A.

Fig. 16 shows the waveforms of the buck mode when $v_i = 200$ V. The driving signal of the switch T_5 is always ON, which shows that the boost ac/ac part does not work. Figs. 17–20 show the comparisons of the experimental waveforms in constant boost ratio modulation and the dual-mode modulation when the input voltage is 100 V. Fig. 17 illustrates the input and output voltage and inductor current in two modulations.

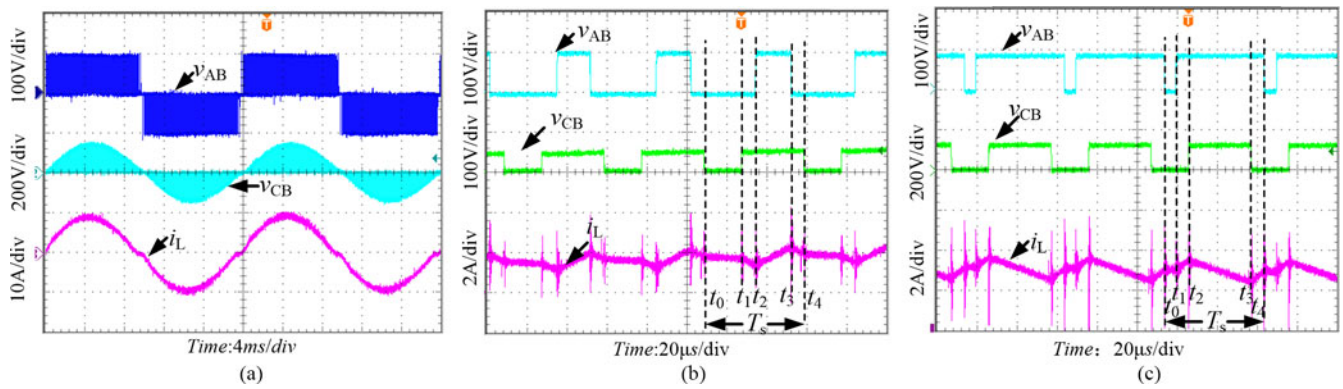

Fig. 19. Voltage and current of the inductor in constant boost ratio modulation. (a) Voltage and current of the inductor. (b) $v_i > v_o$. (c) $v_i < v_o$.

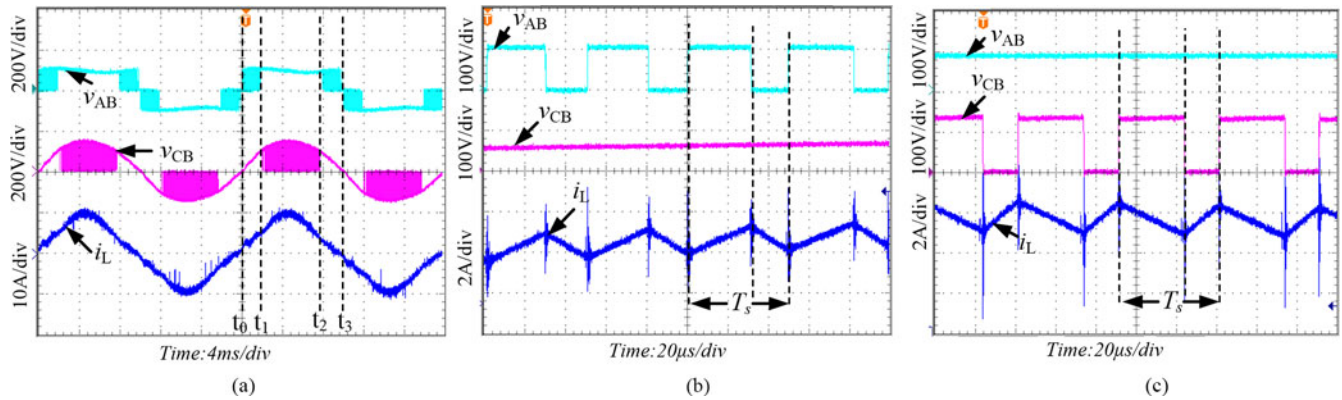

Fig. 20. Voltage and current of the inductor in dual-mode modulation. (a) Voltage and current of the inductor. (b) Buck mode ($v_i > v_o$). (c) Boost mode ($v_i < v_o$).

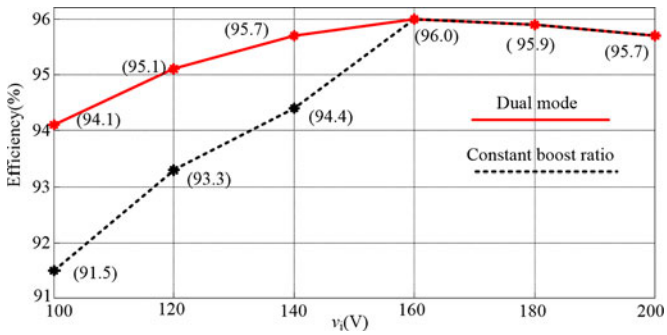

Fig. 21. Efficiency comparison of two modulation strategies.

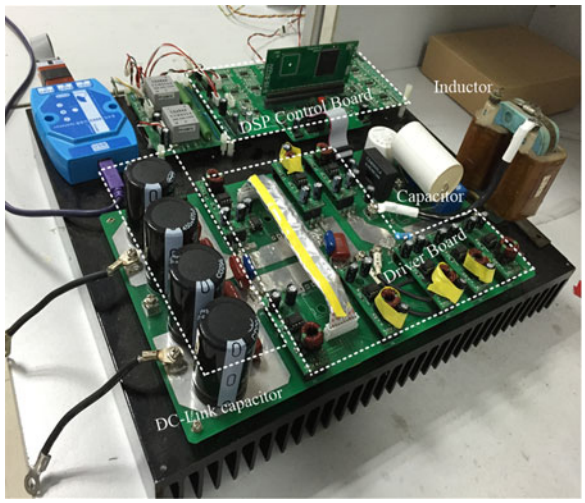

Fig. 22. Prototype picture.

The inductor current in dual-mode modulation is lower than in constant boost ratio modulation. Fig. 18 shows the driving signals of the switches in two modulations. We can see that in dual-mode modulation, the time when the switches operate in high frequency is less than in constant boost ratio modulation. Figs. 19 and 20 show that the inductor current is lower but the ripple is larger in dual-mode modulation. Fig. 21 indicates the efficiency comparison of two modulation strategies, and the prototype picture is shown in Fig. 22. Obviously, when $v_i < V_{\rm op}$, the efficiency of the inverter in dual-mode modulation is higher than in constant boost ratio modulation and the efficiency curve rise with the input voltage; when $v_i > V_{\rm op}$, the inverter is equivalent to the conventional full-bridge inverter in two modulation strategies. So they have the same efficiency, and the efficiency curve drops when the input voltage becomes larger.

VI. Conclusion

This paper has studied a novel inverter, which is suitable for PV, achieving inversion and boosting with a wide range of input. It can help in reducing the system volume and improving the power density when the boost ac/ac structure takes the place of the conventional transformer. Two different modulation strategies can be applied to the inverter: constant boost ratio modulation and the dual-mode modulation. Two modulation methods are analyzed, respectively, and the comparison on the inductor current and the current stress of the switches is made. The result is that the dual-mode modulation can help in improving the system efficiency and reducing the inductor current and the current stress of the switches. Finally, a 100–200-V dc input, 110-V ac output, and 500-W rated power prototype is fabricated and tested experimentally. The results show that the inverter can operate in dual-mode modulation.

References

[1] Y. Bo, L. Wuhua, G. Yunjie, C. Wenfeng, and H. Xiangning, "Improved transformerless inverter with common-mode leakage current elimination for a photovoltaic grid-connected power system," *IEEE Trans. Power Electron.*, vol. 27, no. 2, pp. 752–762, Feb. 2012.

[2] H. S. Kim, M. H. Ryu, J. W. Baek, and J. H. Jung, "High-efficiency isolated bidirectional AC–DC converter for a dc distribution system," *IEEE Trans. Power Electron.*, vol. 28, no. 4, pp. 1642–1654, Apr. 2013.

[3] T. Kerekes, R. Teodorescu, and U. Borup, "Transformerless photovoltaic inverters connected to the grid," in Proc. IEEE 22nd Annu. Appl. Power Electron. Conf., 2007, pp. 1733–1737.

[4] T. A. Huld, M. Suri, R. P. Kenny, and E. D. Dunlop, "Estimating PV performance over large geographical regions," in Proc. IEEE 31st Photovoltaic Spec. Conf., 2005, pp. 1679–1682.

[5] W. Zhu, K. Zhou, and M. Cheng, "A bidirectional high-frequency-link single-phase inverter: Modulation, modeling, and control," *IEEE Trans. Power Electron.*, vol. 29, no. 8, pp. 4049–4057, Aug. 2014.

[6] M. Jang, M. Ciobotaru, and V. G. Agelidis, "A single-stage fuel cell energy system based on a buck–boost inverter with a backup energy storage unit," *IEEE Trans. Power Electron.*, vol. 27, no. 6, pp. 2825–2834, Jun. 2012.

[7] Y. Huang, M. Shen, F. Peng, and J. Wang, "Z-source inverter for residential photovoltaic systems," *IEEE Trans. Power Electron.*, vol. 21, no. 6, pp. 1776–1782, Nov. 2006.

[8] C. Wang, "A novel single-stage full-bridge buck-boost inverter," in Proc. IEEE 18th Annu. Appl. Power Electron. Conf. Expo., 2003. pp. 51–57.

[9] P. G. Barbosa, H. A. C. Braga, and E. C. Teixeira, "Boost current multilevel inverter and its application on single-phase grid-connected photovoltaic systems," *IEEE Trans. Power Electron.*, vol. 21, no. 4, pp. 1116–1124, Jul. 2006.

[10] S. B. Kjaer, J. K. Pedersen, and F. Blaabjerg, "A review of single phase grid-connected inverters for photovoltaic modules," *IEEE Trans. Ind. Appl.*, vol. 41, no. 5, pp. 1292–1306, Sep./Oct. 2005.

[11] W. Yu, C. Hutchens, J.-S. Lai, J. Zhang, G. Lisi, A. Djabbari, G. Smith, and T. Hegarty, "High efficiency converter with charge pump and coupled inductor for wide input photovoltaic ac module applications," in Proc. IEEE Energy Convers. Congr. Expo., 2009, pp. 3895–3900.

[12] L. Chen, A. Amirahmadi, Q. Zhang, N. Kutkut, and I. Batarseh, "Design and implementation of three-phase two-stage grid-connected module integrated converter," *IEEE Trans. Power Electron.*, vol. 29, no. 8, pp. 3881–3892, Aug. 2014.

[13] Z. Zhao, M. Xu, Q. Chen, J.-S. Lai, and Y. Cho, "Derivation, analysis, and implementation of a boost–buck converter-based high-efficiency PV inverter," *IEEE Trans. Power Electron.*, vol. 27, no. 3, pp. 1304–1313, Mar. 2012.

[14] S. Jain and V. Agarwal, "A single-stage grid connected inverter topology for solar PV systems with maximum power point tracking," *IEEE Trans. Power Electron*, , vol. 22, no. 5, pp. 1928–1940, Sep. 2007.

[15] H. Ribeiro, A. Pinto, and B. Borges, "Single-stage DC-AC converter for photovoltaic systems," in Proc. IEEE Energy Convers. Congr. Expo., 2010, pp. 604–610.

[16] Y. Zhou and W. Huang, "Single-stage boost inverter with coupled inductor," *IEEE Trans. Power Electron.*, vol. 27, no. 4, pp. 1885–1893, Apr. 2012.

[17] Y. Li, S. Jiang, J. G. Cintron-Rivera, and F. Zheng Peng, "Modeling and control of quasi-Z-source inverter for distributed generation applications," *IEEE Trans. Power Electron.*, vol. 60, no. 4, pp. 1532–1541, Apr. 2013.

[18] F. Xu, Y. Tang, and Y. He, "Half cycle modulation strategy researches on double boost inverters," *Proc. Chin. Soc. Electr. Eng.*, vol. 340, no. 36, pp. 6407–6414, Dec. 2014.

[19] W. Wu, J. Ji, and F. Blaabjerg, "Aalborg inverter—A new type of "buck in buck, boost in boost" grid-tied inverter," *IEEE Trans. Power Electron.*, vol. 30, no. 9, pp. 4784–4793, Sep. 2015.

[20] Y. Tang, X. Dong, and Y. He, "Active buck-boost inverter," *IEEE Trans. Ind. Electron.*, vol. 61, no. 9, pp. 4691–4697, Sep. 2014.

[21] K. Ogura, T. Nishida, E. Hiraki, M. Nakaoka, and S. Nagai, "Time-sharing boost chopper cascaded dual mode single-phase sinewave inverter for solar photovoltaic power generation system," in Proc. Power Electron. Spec. Conf., 2004, pp. 4763–4767.

[22] W. Xu, H. Qin, B. Zhou, H. Xue, and L. Yang, "A novel time-sharing dual-mode control strategy in cascaded sinusoidal inverter," in Proc. 7th Power Electron. Motion Control Conf., 2012, pp. 820–825.

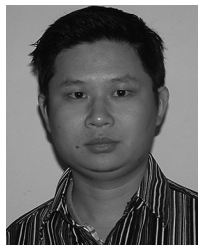

Yu Tang (M'09) received the B.S. and Ph.D. degrees both in electrical engineering from the Nanjing University of Aeronautics and Astronautics (NUAA), Nanjing, China, in 2003 and 2008, respectively.

Since 2008, he has been with the Electrical Engineering Department at NUAA and is currently an Associate Professor. He has published more than 30 papers in journals and conference proceedings, and hold two china patents. His research interest includes power electronics in renewable energy generation.

Fei Xu (S'15) was born in China in 1989. He received the B.S. degree from the College of Electrical Engineering and Automation, Anhui University, Hefei, China, in 2013. He is currently working toward the M.S. degree at the College of Automation Engineering, Nanjing University of Aeronautics and Astronautics, Nanjing, China.

Yang Bai was born in China in 1992. He received the B.S. degree from the College of Electrical Engineering and Automation, Anhui University, Hefei, China, in 2014. He is currently working toward the M.S. degree at the College of Automation Engineering, Nanjing University of Aeronautics and Astronautics, Nanjing, China.

Yaohua He was born in China in 1990. He received the B.S. degree from the Department of Electrical Engineering, Anhui University of Science and Technology, Huainan, China, in 2012, and the M.S. degree from the College of Automation Engineering, Nanjing University of Aeronautics and Astronautics, Nanjing, China, in 2015.